


High-field quantum spin liquid transitions and angle-field phase diagram of the Kitaev magnet α -RuCl₃

Han Li^{1,2}, Wei Li^{1,2,*} and Gang Su^{1,2,†}

¹Kavli Institute for Theoretical Sciences, University of Chinese Academy of Sciences, Beijing 100190, China

²CAS Center for Excellence in Topological Quantum Computation, University of Chinese Academy of Sciences, Beijing 100190, China

³CAS Key Laboratory of Theoretical Physics, Institute of Theoretical Physics, Chinese Academy of Sciences, Beijing 100190, China

 (Received 3 November 2022; revised 1 February 2023; accepted 2 February 2023; published 10 March 2023)

The pursuit of quantum spin liquid (QSL) in the Kitaev honeycomb magnets has drawn intensive attention recently. In particular, α -RuCl₃ has been widely recognized as a promising candidate for the Kitaev QSL. Although the compound exhibits an antiferromagnetic order under zero field, it is believed to be endowed with fractionalized excitations and can be driven to the QSL phase by magnetic fields. Here, based on a realistic K - J - Γ - Γ' model for α -RuCl₃, we exploit the exponential tensor renormalization group approach to explore the phase diagram of the compound under magnetic fields. We calculate the thermodynamic quantities, including the specific heat, Grüneisen parameter, magnetic torque, magnetotropic susceptibility, and so on, under a magnetic field with a tilting angle θ to the c^* -axis perpendicular to the honeycomb plane. We find an extended QSL in the angle-field phase diagram determined with thermodynamic responses. The gapless nature of such field-induced QSL is identified from the specific heat and entropy data computed down to very low temperatures. The present study provides guidance for future high-field experiments for the QSL in α -RuCl₃ and other candidate Kitaev magnets.

DOI: [10.1103/PhysRevB.107.115124](https://doi.org/10.1103/PhysRevB.107.115124)

I. INTRODUCTION

Quantum spin liquids (QSL) constitute an exotic many-body state without symmetry-breaking spin order, where a number of unconventional properties such as fractionalized excitations and long-range entanglement emerge [1–5]. The celebrated, exactly solvable Kitaev model has attracted enormous attention due to the QSL ground state with localized and itinerant Majorana fermions useful for fault-tolerant quantum computing [6,7]. Such remarkable properties incited a flurry of works on the materialization of the Kitaev model in, e.g., certain $4d$ - and $5d$ -electron compounds including cations with the low-spin d^5 electron configuration and the edge-shared ligand octahedra. It yields the Kitaev interaction by the synergy of large spin-orbit coupling and Coulomb repulsion on a honeycomb lattice [8]. Moreover, some high-spin d - and f -electron systems beyond the Jackeli-Khaliullin mechanism have come forth recently which may also realize the Kitaev interaction in the compounds [9–12].

The ruthenium halide α -RuCl₃ is arguably the most studied Kitaev material [13–29]. Although it has a long-range zigzag antiferromagnetic ordered state below 7 K [13–15], proximate Kitaev QSL behaviors at elevated temperatures were observed [15,16]. The zigzag spin order is suppressed under an in-plane field of around 7 T [16–19], where the possible field-induced QSL phase was intensively studied via multiple experimental probes in-

cluding the Raman scattering [22], terahertz absorption measurements [23], nuclear magnetic resonance [19–21], magnetic torque [24,25], and thermal Hall conductivity measurements [26–29].

On the other hand, in the theoretical studies, the accurate microscopic model description of α -RuCl₃ is important for understanding the compound, which, however, has been unsettled for a long period [31]. Recently, some of the authors proposed a Kitaev-Heisenberg-Gamma-Gamma' (K - J - Γ - Γ') model with dominant Kitaev interaction $K = -25$ meV, nearest-neighbor Heisenberg coupling $J = -0.1|K|$, off-diagonal terms $\Gamma = 0.3|K|$, and $\Gamma' = -0.02|K|$, which puts the major experimental observations in a coherent picture and makes a relevant prediction of QSL states induced by high out-of-plane fields [32]. Such a high-field QSL phase is separated from zigzag antiferromagnetic and the polarized phases, through two quantum phase transitions (QPTs) at 35 T and 130 T, respectively. This theoretical prediction was recently confirmed in high pulsed field experiments [30].

In this work, we extend the previous theoretical studies to the angle-field phase diagram of the realistic K - J - Γ - Γ' model with the thermal tensor network approach [33–35]. Through the finite-temperature simulations of the specific heat C_m , Grüneisen parameters Γ_B , magnetic torque τ , magnetotropic susceptibility k , and so on, we find a high-field QSL phase residing between the zigzag antiferromagnetic and the field-polarized phases. We determine the transition fields with prominent thermodynamic responses and offer concrete theoretical proposal for experimental probes of such spin liquid transitions in α -RuCl₃ and potentially also other Kitaev candidate magnets.

*w.li@itp.ac.cn

†gsu@ucas.ac.cn

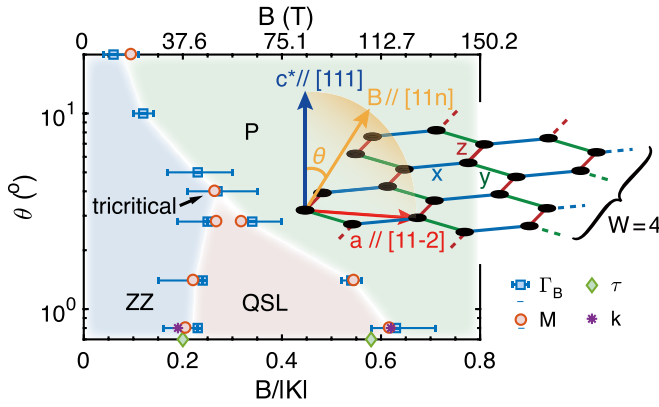


FIG. 1. The angle-field phase diagram of the realistic K - J - Γ - Γ' model for α - RuCl_3 . There are three phases including zigzag (ZZ), quantum spin liquid (QSL), and the polarized (P) states as indicated in the figure. The phase boundaries are determined from the responses in Grüneisen parameters Γ_B , magnetic torque τ , and the magnetotropic susceptibility k at $T/|K| \simeq 0.01$, consistent with that from the ground-state magnetization curves [30]. We reveal that the phase transitions between ZZ (a “solid” order), QSL (liquid-like phase), and the P (a weakly interacting “gas”-like system) phases meet at a tricritical point. The inset illustrates the honeycomb lattice defined on a cylinder of width $W = 4$, where the x , y , and z bonds with bond-directional Kitaev interactions are marked in blue, green, and red colors, respectively. The in-plane a -axis, out-of-plane c^* -axis, and the angle θ of the applied field within the ac^* -plane are indicated by the arrows.

II. MODEL AND METHODS

The effective spin Hamiltonian of α - RuCl_3 [32] considered in this work reads

$$H = \sum_{\langle i, j \rangle_\gamma} [K S_i^\alpha S_j^\alpha + J \mathbf{S}_i \cdot \mathbf{S}_j + \Gamma (S_i^\alpha S_j^\beta + S_i^\beta S_j^\alpha) + \Gamma' (S_i^\alpha S_j^\alpha + S_i^\alpha S_j^\beta + S_i^\beta S_j^\alpha + S_i^\beta S_j^\beta)], \quad (1)$$

where the summation is over the nearest-neighbor (NN) bond $\langle i, j \rangle_\gamma$ with $\gamma = \{x, y, z\}$ (see inset in Fig. 1). K denotes the bond-dependent Kitaev interactions, J is the Heisenberg term, and Γ, Γ' are the off-diagonal symmetric couplings with $\{\alpha, \beta, \gamma\}$ being the three spin components under a cyclic permutation.

The magnetic field B is applied along the direction $[l \ m \ n]$ in the spin space (S^x, S^y, S^z) , i.e., the Zeeman term is $H_{\text{Zeeman}} = \frac{B}{\sqrt{l^2+m^2+n^2}} [S^x, S^y, S^z] \cdot [l, m, n]^T$. Therefore, $H_{[11\bar{2}]}$ and $H_{[111]}$ correspond to the fields applied along the a - and c^* -axes, respectively. The angle between the applied field $H_{[11n]}$ and c^* -axis within the ac^* -plane can be represented by $\theta = \arccos(\frac{2+n}{\sqrt{6+3n^2}}) \times \frac{180^\circ}{\pi}$, as depicted in the inset of Fig. 1.

Simulations based on the K - J - Γ - Γ' model can well reproduce the low-temperature zigzag order [13–15], double-peaked specific heat [15,36,37], magnetic anisotropy [13,14,36,38–41], magnetization curves [16,19,36,38], and the prominent M-star dynamical spin structure factors [14,15] in α - RuCl_3 (see a brief recapitulation in Appendix A). Besides, one remarkable prediction based on this realistic model is the presence of

high-field QSL driven by out-of-plane fields [32] whose nature is still under intensive investigation [42].

Below we employ the exponential tensor renormalization group (XTRG) [34,35] method and perform finite-temperature calculations on a honeycomb-lattice cylinder with total sites $N = W \times L \times 2$, where the width is fixed as $W = 4$ and length L ranges from 6 to 12, as illustrated in the inset of Fig. 1. We retained up to $D = 400$ bond states with truncation errors $\epsilon \simeq 10^{-4}$ down to the lowest temperature $T/|K| \simeq 0.0085$, which guarantees well-converged results till the lowest temperature (cf. Appendix B).

III. FINITE-TEMPERATURE CHARACTERISTICS OF QUANTUM SPIN STATES AND TRANSITIONS

A. Specific heat and isentropes

We start with conventional thermodynamic quantities such as the specific heat C_m and magnetic entropy $S/\ln 2$ in Figs. 2(a) to 2(d), where the contour plots can be used to map the temperature-field phase diagram with various angles θ . As shown in Fig. 2(a), when the field is applied along the $\theta = 0.8^\circ$ direction, the double-peaked C_m structure can be observed under a finite range of fields ($B/|K| \lesssim 0.22$), with the high- T and low- T peaks correspond to two temperature scales T_H and T_L : the short-range spin correlations establish at T_H and the long-range antiferromagnetic zigzag order is formed below T_L , respectively. When the field $B/|K|$ is increased from 0 to 0.22, the low- T C_m peak moves towards lower temperatures, indicating that the zigzag order gets gradually suppressed by the magnetic fields. On the other hand, as the field exceeds $B/|K| = 0.22$, and below the polarization field, a low- T peak emerges as indicated by T_L'' , below which there exists a field-induced QSL phase (cf. Appendix A).

It is noteworthy to mention that above T_L'' , and below the high- T scale T_H , there emerges an intermediate-temperature regime strongly influenced by the Kitaev interactions [43–47], dubbed the Kitaev fractional liquid (KFL). For the original Kitaev model, the KFL regime arises as, in the parton language, the itinerant Majorana fermions move in the background of strongly fluctuating Z_2 fluxes, where the bond-directional, short-range spin correlations were established, while the Z_2 fluxes are disordered [43–47]. Such a KFL regime has universal thermodynamic traits, including the metallic linear specific heat, the fractional magnetic entropy, the emergent Curie-law susceptibility, and so on [44,47]. The KFL behaviors are robust and were observed at intermediate temperature for the realistic K - J - Γ - Γ' model under out-of-plane fields along the c^* axis [32]. Here, as indicated in Figs. 2(a) and 2(b) we find that the KFL behaviors are also present under tilted fields (see more details in Appendix A).

The corresponding isentropes with $\theta = 0.8^\circ$ are shown in Fig. 2(c). The adiabatic T - B curves exhibit distinct changes when entering (rapid increase of T) and leaving (a dip) the intermediate QSL regime. They clearly signal two QPTs from the zigzag order to the QSL phase then to the field-polarized phases, at $B/|K| \simeq 0.22$ and 0.62 , respectively. The transition fields determined with density matrix renormalization group (DMRG) calculations on the same geometry [30] are denoted

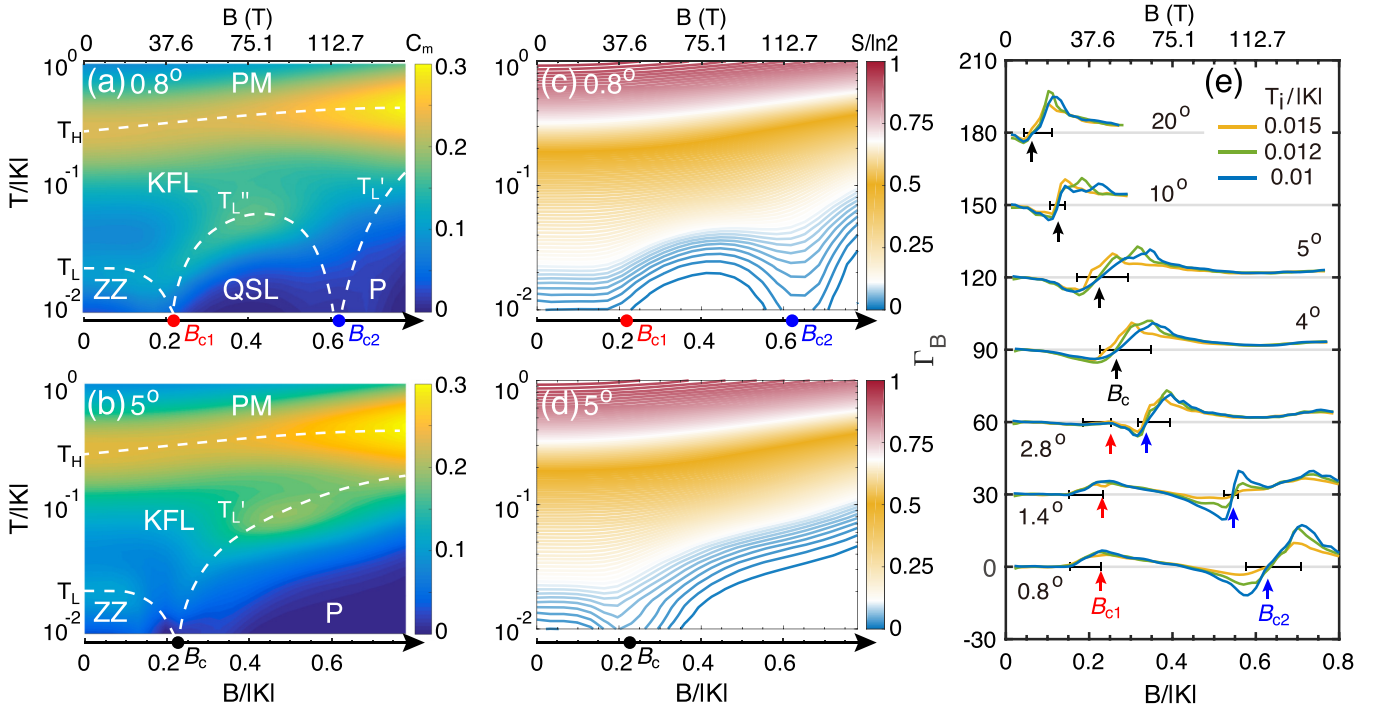


FIG. 2. (a), (b) Contour plots of the specific heat results in fields applied along $\theta = 0.8^\circ$ and 5° , respectively. The solid dots marked on the $T = 0$ axis denote the QPTs obtained through the DMRG calculations [30]. The white dashed lines separating the ZZ, QSL, P, Kitaev fractional liquid (KFL), and paramagnetic (PM) phases are schematic and guides for the eyes (cf., Appendix A for the determination of the temperature scales). (c), (d) The isentropes $S/\ln 2$ for two different θ angles, where the critical fields ($B_{c1,c2}$ and B_c) are indicated by the dots. These calculations with scanned fields are performed on the $YC4 \times 6 \times 2$ lattice. (e) The field-dependent Grüneisen parameters Γ_B at various θ angles with fixed initial temperatures $T_i \simeq 0.015, 0.012$, and 0.01 . The data are calculated by $\Gamma_B = 1/T(dT/dH)_S$, and are shifted vertically by a value of 30 for clarity. For small θ , e.g., $0.8^\circ, 1.4^\circ$, and 2.8° , two critical fields B_{c1} and B_{c2} indicated by the red and blue arrows denote the low- and high-field phase transitions, respectively; while only a single phase transition B_c indicated by a black arrow is observed for $\theta \geq 4^\circ$. The segment around each arrow gives the range of error bar for the determined transition fields.

in the $T = 0$ axis with solid dots, where excellent agreements with the present finite-temperature results are seen.

The situation changes dramatically when the field angle increases to $\theta = 5^\circ$. As shown in Figs. 2(b) and 2(d), the results suggest that there is only one critical field between the zigzag ordered and field polarized phases, with no intermediate states any more. The behaviors of C_m and S are quite similar to that of the in-plane-field case [32], except that the transition field is higher. Thus we find the intermediate QSL phase very sensitively depends on the angle θ . To accurately determine the phase boundaries in the angle-field phase diagram, below we resort to the thermodynamic, experimentally accessible quantities and parameters.

B. Grüneisen parameter

The magnetic Grüneisen parameter Γ_B was employed to accurately determine the critical in-plane fields in α - RuCl_3 [48], which, however, poses challenges to many-body calculations. Here with the state-of-the-art XTRG method, we are able to compute this thermodynamic ratio and show the results in Fig. 2(e). The field-dependent $\Gamma_B = 1/T(dT/dH)_S$ are derived from the simulated isentropes starting from various initial temperatures (and a fixed field). A sign change structure in Γ_B can be observed in Fig. 2(e) near the higher transition field $B_{c2}/|K| \simeq 0.62$ (indicated by

the blue arrows) and it becomes more and more pronounced as temperature lowers, revealing a second-order phase transition from QSL to the polarized phase. On the other hand, in the relatively low-field regime with $B_{c1}/|K| \simeq 0.22$, a peak in Γ_B is observed (indicated by a red arrow) that corresponds to a first-order QPT between ZZ and the QSL phases.

When the field is rotated within the ac^* -plane, the higher transition field shifts from $B/|K| \simeq 0.62$ to 0.06 as the angle θ changes from 0.8° to 20° , which reflects that the polarization field is very sensitive to the angle θ . The first-order QPT stays around $B_{c1}/|K| \simeq 0.23$ for small angles and merges to the second-order QPT at around $\theta \geq 4^\circ$, where a tricritical point emerges. In Fig. 1, we gather the transition fields estimated by Γ_B and obtain the angle-field phase diagram. As also indicated in Fig. 2(e), the error bars of the phase boundaries can be estimated as the difference in field strengths of the dips and peaks in Γ_B .

C. Magnetic torque and magnetotropic susceptibility

The torque magnetometry constitutes a sensitive technique to probe the magnetic anisotropies in quantum materials and recently was used to study the intricate quantum spin states and transitions in α - RuCl_3 [25,49]. However, its numerical results are lacking, partly due to the challenges in its many-body simulations.

With thermal tensor networks, we can compute the magnetic torque and its derivative, magnetotropic susceptibility, with a high accuracy. As the free energy F can be written as $dF = -SdT - PdV - MdB + \tau d\theta$ where θ is the tilted angle of the magnetic field, the first derivative $\tau = \partial F / \partial \theta$ represents the magnetic torque, which can be measured in α -RuCl₃ experiments through $M \times B$ [49]. Recently, resonant torsion magnetometry technique was also used to measure the magnetotropic susceptibility $k = \partial^2 F / \partial \theta^2$ (the second derivative of free energy) [25,50]. Following this line, below we perform XTRG calculations of the K - J - Γ - Γ' model for α -RuCl₃, investigate τ and k at various temperatures and fields, and predict salient features of the two QPTs in the magnetotropic quantities to be checked in future high-field measurements.

In Fig. 3(a), we show the magnetic torque $\tau(\theta/2) = (F_\theta - F_0)/\theta$ (where F_0 represents the free energy at zero field) with $\theta = 0.8^\circ$ and 1.4° computed at low temperatures $T/|K| = 0.03, 0.02$, and 0.01 . At low fields, $B < B_{c1}$, we find a relatively small value of τ , which is understandable as the torques in two sublattices are expected to cancel each other in the antiferromagnetic ZZ phase, resulting in a nearly zero total net torque value. As the fields further increase, the calculated τ gets enhanced rapidly as the ZZ order is suppressed in the intermediate QSL regime, which eventually drops again to small values at high fields as the system enters to the polarized phase. This can be ascribed to the fact that the angle between induced moments and fields is almost zero. The transition fields can thus be determined from where the torque changes most rapidly by computing the derivatives of τ with respect to the field B , i.e., $d\tau/dB$ shown in Fig. 3(a). The red and blue arrows indicate the transition fields from ZZ to QSL and QSL to the polarized phases, respectively.

The behaviors of magnetic torque are also found to be consistent with the static spin-structure factor results

$$S(\mathbf{k}) = \sum_{j \in N, j \neq i_0} e^{i\mathbf{k}(\mathbf{r}_j - \mathbf{r}_{i_0})} (\langle S_{i_0} S_j \rangle - \langle S_{i_0} \rangle \langle S_j \rangle), \quad (2)$$

where i_0 indicates a central reference site and the results are at relatively low temperature $T/|K| \simeq 0.02$ and 0.01 . As shown in Fig. 3(b), the zigzag spin correlations at small fields, e.g., $B < B_{c1}$ can be evidenced by the large $S(M)$ value [with the M as well as Γ point indicated in the inset of Fig. 3(b)], which becomes suppressed in the intermediate QSL phase. The enhancement of $S(\Gamma)$ near B_{c1} signals the buildup of uniform magnetization where the torque τ also increases rapidly in Fig. 3(a). When the system enters the spin polarized phase at B_{c2} , the structure factor peaks at M and Γ points both vanish as expected [Fig. 3(b)].

The magnetotropic susceptibility k can also be used to sensitively probe the two quantum phase transitions. In Fig. 3(c), we plot the results with $\theta = 0.8^\circ$ at $T/|K| = 0.03, 0.02$, and 0.01 . The parameter k , second-order derivative of the free energy with respect to the magnetic field orientation θ , has an intimate relation to the susceptibility χ [50] and exhibits discontinuities at second-order phase transitions. In Fig. 3(c), the sharp dip at around $B \simeq B_{c2}$ denoted by the blue arrow corresponds to a second-order transition, while the low-field one, as emphasized in the inset, shows a kink at around

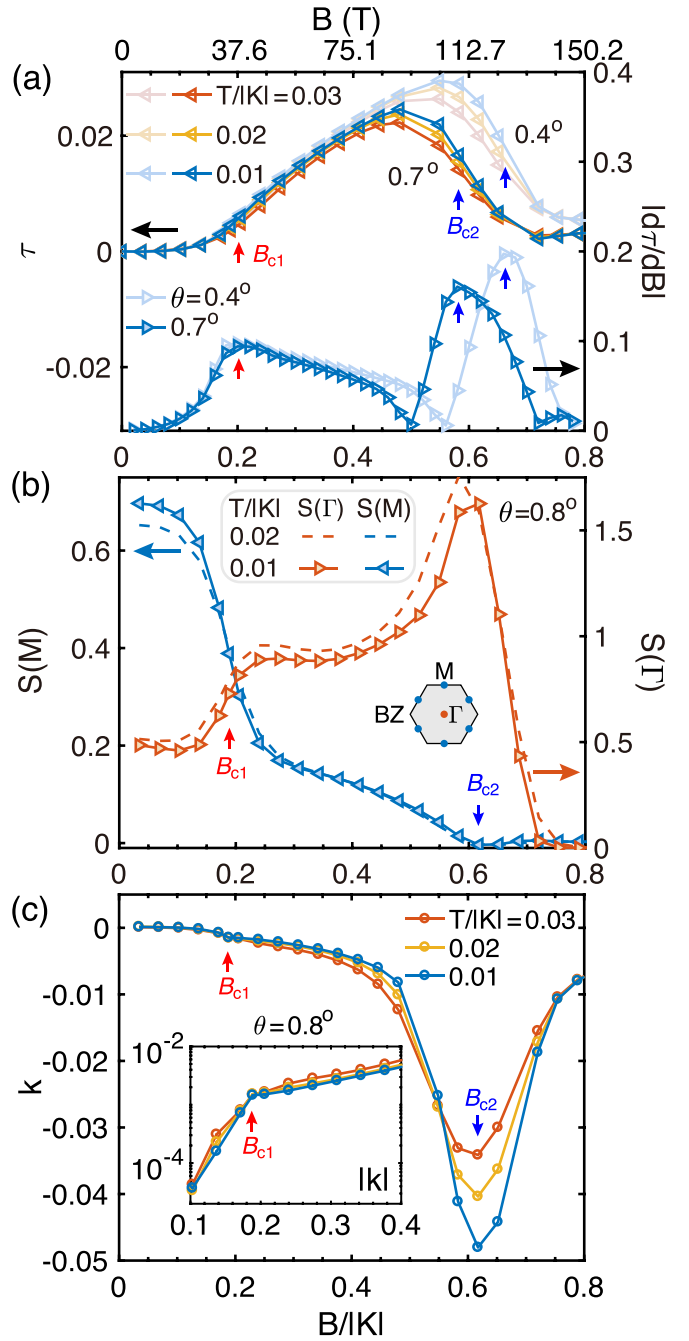


FIG. 3. (a) The calculated magnetic torque τ (the upside curves with left axis) and the absolute value of its derivative $|d\tau/dB|$ (the downside two with right axis) of α -RuCl₃ model with fields applied along $\theta = 0.4^\circ$ and 0.7° at $T \simeq 0.03, 0.02$, and 0.01 . Two transition fields B_{c1} and B_{c2} are identified from the peak positions of $|d\tau/dB|$ indicated by the red and blue arrows, respectively. (b) The static spin-structure factors $S(\mathbf{k})$ (see the main text) for $\theta \simeq 0.8^\circ$ with $\mathbf{k} = M$ and Γ in the Brillouin zone (shown in the inset). The red arrow denotes a fast drop of $S(M)$, indicating the suppression of the zigzag antiferromagnetic order at low temperatures, while the blue arrow corresponds to the field where both $S(M)$ and $S(\Gamma)$ decrease towards zero. (c) The calculated magnetotropic susceptibility k for $\theta \simeq 0.8^\circ$ at various low temperatures. The sharp dip corresponds to the second-order phase transition denoted by the blue arrow, while a kink occurs at around $B/|K| = 0.19$ signposted by the red arrow as zoomed in in the inset.

$B \simeq B_{c1}$ which corresponds to a first-order phase transition. From the magnetotropic quantities τ and k , we determine the transition fields at $\theta = 0.7^\circ$ and 0.8° and show them also in Fig. 1. Besides, we also computed the matrix product operator (MPO) entanglement of the system, which provided an accurate estimate of transition fields in accordance with the results above (see Appendix C). With these finite-temperature simulations, we show that the high-field torque magnetometry measurements can be used to sensitively detect the two QPTs associated with the intermediate QSL phase in future experimental studies.

IV. GAPLESS NATURE OF THE HIGH-FIELD QSL IDENTIFIED FROM THERMODYNAMICS

As indicated by the dome-like feature in Figs. 2(a) and 2(c), there exist an intermediate QSL regime below the emergent low-temperature scale T_L'' . To further reveal the nature of this intermediate phase, we push the calculations of C_m and $S/\ln 2$ to longer YC4 cylinders with L up to 12.

In Fig. 4(a), we find the high- and low-temperature scales T_H and T_L'' change only slightly as we elongate the system from $L = 6$ to $L = 12$. The height of the peak at T_L'' gets lowered, while the C_m values for $T < T_L''$ are actually enhanced, which gives rise to a shoulder-like structure for the largest system size $L = 12$ as indicated by the grey arrow below $T/|K| \simeq 0.03$. The corresponding entropy curves are shown in Fig. 4(b), where we see that there are a considerable amount of low-temperature entropies below $T/|K| \simeq 0.03$, indicating the strong spin fluctuations and large spin excitation density of states. In the inset of Fig. 4(b), we subtract the results of two YC4 lattices with different (adjacent) lengths, e.g., the [8-6] represent results obtained by subtracting YC4 $\times 6 \times 2$ data from the YC4 $\times 8 \times 2$. The obtained entropy results reflect the bulk property in the central columns and suffer less severe boundary effects, and a power-law behavior of entropy $S \sim T^\alpha$ can be clearly seen, which indicates that the high-field QSL has gapless low-energy excitations and there are considerable entropies released only below the temperature $T \simeq 0.03|K|$. Overall, the thermodynamic results here along the tilted angle point to the conclusion of a gapless QSL, consistent with previous DMRG results (restricted to out-of-plane fields) [32].

V. CONCLUSION AND DISCUSSIONS

In the present work, we calculated the experimentally relevant thermodynamic properties, i.e., magnetic specific heat, magnetocaloric effect characterized by the Grüneisen parameters, magnetic torque, and the magnetotropic susceptibility of the primary candidate Kitaev magnet α -RuCl₃ based on the realistic K - J - Γ - Γ' model and through the highly accurate XTRG method. Recently, a high-field magnetization measurement on α -RuCl₃ up to 102 T witnessed two phase transitions enclosing an intermediate phase [30], in agreement with the prediction based on the model calculations [32]. Here we calculated further thermodynamic properties that provide a comprehensive angle-field phase diagram and useful guide for future experimental studies. For $\theta < 4^\circ$, we find two field-induced quantum phase transitions evidenced by var-

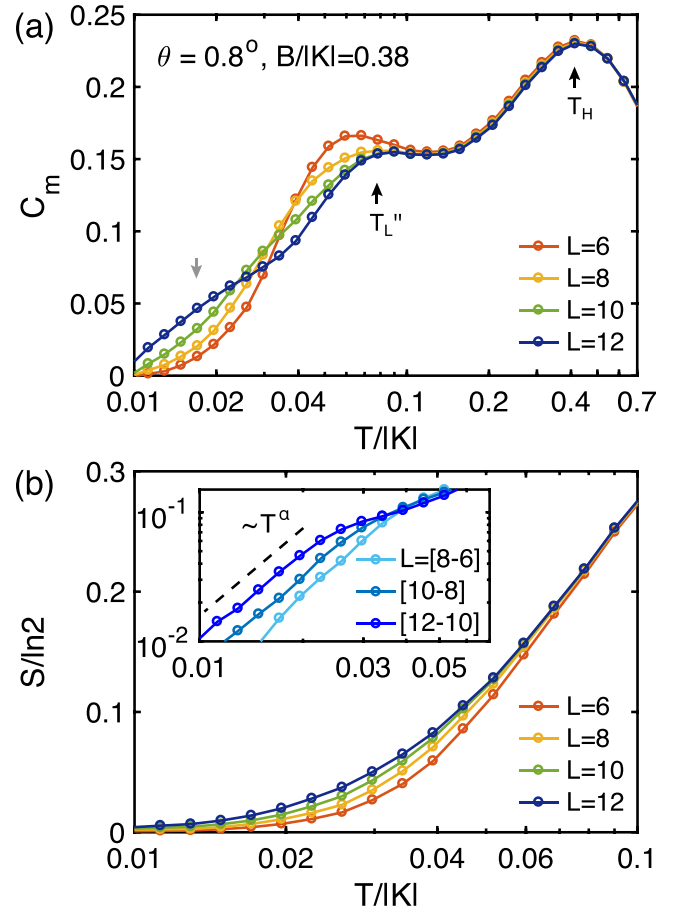


FIG. 4. (a) The computed specific heat C_m on various YC4 $\times L \times 2$ geometries with different lengths L ranging from 6 to 12 under a field $B/|K| = 0.38$ along $\theta = 0.8^\circ$ away from the c^* -axis. The high- and low-temperature scale T_H and T_L'' are indicated. The grey arrow stress the enhancement of C_m at very low temperature $T/|K| < 0.03$ as system length L increases. (b) The corresponding thermal entropy $S/\ln 2$ results, with the subtracted data reflecting the bulk property at low temperature shown in the inset. The dashed line at $T/|K| < 0.02$ represents a power-law fitting with $\alpha \simeq 1.5$, serving as a guide for the eye.

ious quantities. (i) The diverging Grüneisen parameter Γ_B shows a sign change behavior at high-field transition point B_{c2} , suggesting a second-order phase transition. Exactly at the same field, the magnetotropic susceptibility k features a sharp peak. (ii) The hump in Γ_B at around B_{c1} reflects a quantum phase transition possibly of first-order. There is also a peak in $|d\tau/dB|$ and a kink in k , which point to the same conclusion. On the other hand, for large $\theta \gtrsim 4^\circ$, only a single phase transition from antiferromagnetic to polarized phase is found, suggesting the absence of an intermediate QSL phase.

Moreover, it is noteworthy that, besides the conventional candidate materials with Kitaev interactions, e.g., $X_2\text{IrO}_3$ ($X = \text{Na, Li, Cu}$) [51–59], $X_3\text{LiIr}_2\text{O}_3$ ($X = \text{Ag, Cu, H}$) with Ir^{4+} [60–62], XR_3 ($X = \text{Ru, Yb, Cr; R} = \text{Cl, I, Br}$) [56,63–78], and so on, some newly reported Kitaev family such as rare-earth chalcogenide REChX ($\text{RE} = \text{rare earth; Ch} = \text{O, S, Se, Te; X} = \text{F, Cl, Br, I}$) [79,80] cobalt honeycomb oxides $\text{Na}_2\text{Co}_2\text{TeO}_6$ [81,82], $\text{Na}_3\text{Co}_2\text{SbO}_6$ [83],

BaCo₂(AsO₄)₂ [84], and so on, also offer a platform exhibiting highly anisotropic, bond-dependent exchange couplings. It would be worthwhile to explore their field-induced quantum spin states along the out-of-plane direction and generally tilted angles in the future and the present study on angle-field phase diagram of the K - J - Γ - Γ' model provides theoretical guide for experimental explorations in these intriguing quantum magnets.

ACKNOWLEDGMENTS

This work was supported by the National Natural Science Foundation of China (Grants No. 12222412, No. 11974036, No. 11834014, and No. 12047503), Strategic Priority Research Program of the Chinese Academy of Sciences of CAS (Grant No. XDB28000000), National Key R&D Program of China (Grant No. 2018YFA0305800), CAS Project for Young Scientists in Basic Research (Grant No. YSBR-057), and China National Postdoctoral Program for Innovative Talents (Grant No. BX20220291). H.L. and W.L. are indebted to Xu-Guang Zhou, Shun-Yao Yu, Shou-Shu Gong, and Zheng-Xin Liu for stimulating discussions and thank the HPC-ITP for the technical support and generous allocation of CPU time.

APPENDIX A: REALISTIC α -RuCl₃ MODEL AND FIELD-INDUCED PHASES

In the strongly correlated transition metal compounds, α -RuCl₃ is believed to serve as a prototypical candidate material for the Kitaev model [13,14,38,41,68,71,85]. As it undergoes a magnetic transition to antiferromagnetic order at a relatively low temperature, i.e., $T \simeq 7$ K [13,14,36,38], research has taken efforts to find out the effective spin Hamiltonian of α -RuCl₃, which includes not only the Kitaev term K , but also the Heisenberg interactions J , J_2 , and J_3 , and off-diagonal Γ and Γ' couplings [56,63–72,86–88], which is important for gaining insights into the candidate Kitaev material. The Kitaev interaction in this compound has been widely accepted to be ferromagnetic [15,41,56,63–70,89]. However, the magnitudes of K and even the signs of non-Kitaev terms were undetermined and it is very challenging to find a model that can accurately describe the realistic α -RuCl₃ [31].

We focus on the minimal K - J - Γ - Γ' model [32,86,90,91], especially on its field-induced properties. In our previous work [32], we determine the parameters from fitting the thermodynamic properties, i.e., the double-peak feature of specific heat with two temperature scales at around 100 K and 7 K [15,36,37] and the anisotropic susceptibilities along the a - and c^* -axes [14,39,40]. The determined parameter set is $K = -25$ meV, $\Gamma = 0.3|K|$, $\Gamma' = -0.02|K|$, $J = -0.1|K|$, with an in-plane and out-of-plane Landé factor $g_a = 2.5$ and $g_{c^*} = 2.3$, respectively. With this model, the low-temperature zigzag antiferromagnetic order [14] and its magnetization curve can be well reproduced, which are found in quantitative agreement with experiments [36,38]. The transition fields that suppressed the zigzag order are also in accordance with experimental observations, along the in-plane direction [16,19,36,38] and with a tilted $\theta = 35^\circ$ angle [20]. Besides, it was also found that the zigzag order gets suppressed at 35 T under out-of-plane fields ($\theta = 0^\circ$), above which, and below a polarization field of

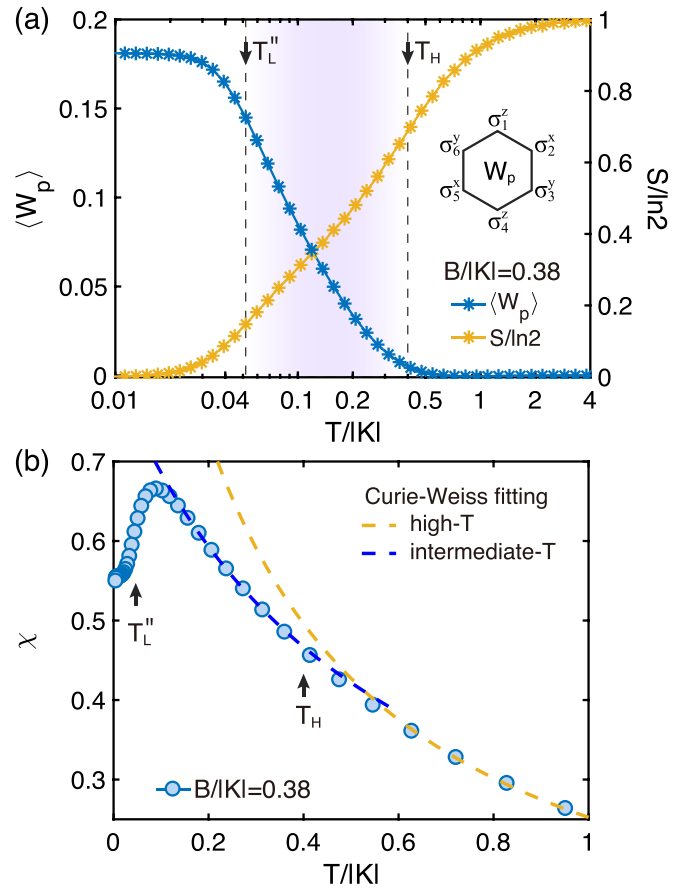


FIG. 5. Finite-temperature quantities including (a) expectation value of plaquette operator W_p , fractional entropy $S/\ln 2$, and (b) emergent Curie-Weiss susceptibility χ are shown. The results are computed with the realistic K - J - Γ - Γ' model on $YC4 \times 6 \times 2$ lattices, under a field $B/|K| = 0.38$ tilted by an angle of $\theta = 0.8^\circ$. In panel (a), the entropy releases rapidly at T_H and T_L'' , corresponding to the two temperature scales as indicated by the arrows. The expectation value $\langle W_p \rangle$ arises at T_H and starts to converge at around T_L'' . In panel (b), we show the high- and intermediate-temperature Curie-Weiss fittings $C/(T + \theta)$ where the constants are determined as $C \simeq 0.31$, $\theta \simeq -0.22$ (for high- T) and $C \simeq 0.44$, $\theta \simeq -0.54$ (intermediate- T), respectively.

100 T level, a field-induced QSL phase emerges as evidenced by both density matrix renormalization group (DMRG) and variational Monte Carlo (VMC) method at ground state [32]. In this work, we further extend the conclusion that the high-field QSL phase can extend to a finite range of θ angles.

At finite temperature, the Kitaev fractional liquid (KFL) regime (also dubbed as “fractional paramagnetic,” “Kitaev paramagnetic,” or “Majorana metal” regime [43–46]) arises as an emergent novel paramagnetic state in not only the original Kitaev honeycomb model but also in the extended Kitaev models at finite temperature [32,47]. In the KFL regime, the short-range spin correlations are established while the Z_2 fluxes remain disordered, each carrying one-half of the total entropies. In Fig. 5, we show the expectation value of plaquette operator $W_p = \sigma_1^z \sigma_2^x \sigma_3^y \sigma_4^z \sigma_5^x \sigma_6^y$ [with σ^γ the Pauli matrix and the subscripts denote the six vertices of a hexagon, see the inset of Fig. 5(a)], thermal entropy S ,

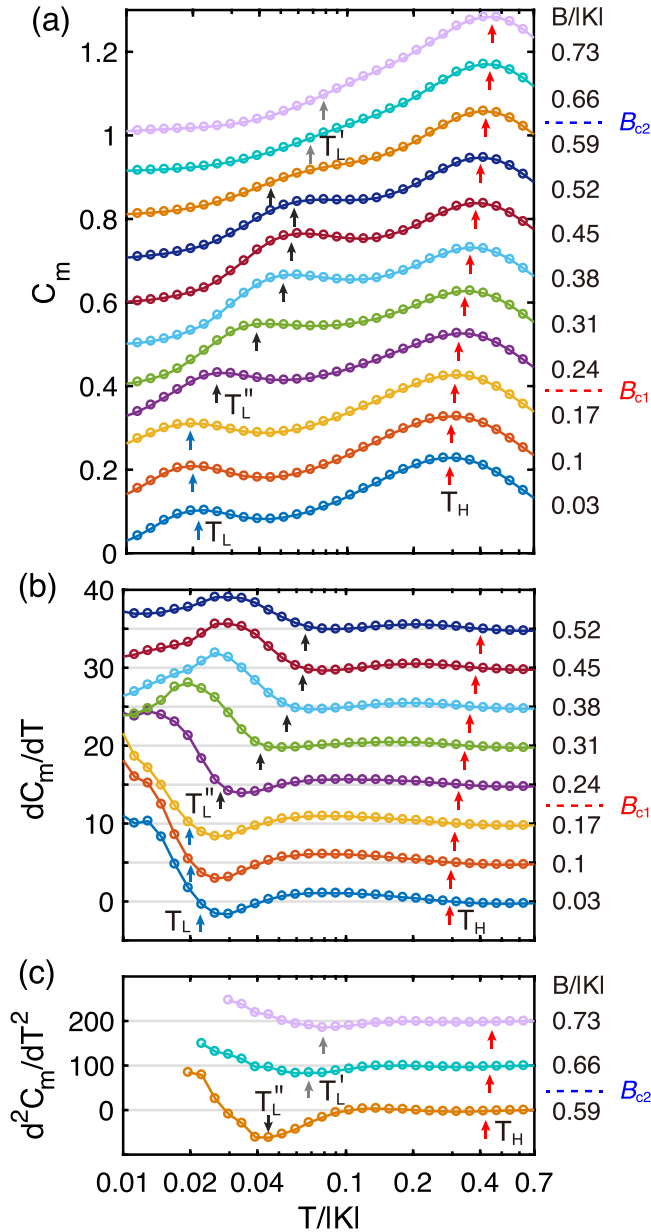


FIG. 6. The temperature-dependent specific heat curves (a) C_m and their first- and second-order derivatives (b) dC_m/dT and (c) d^2C_m/dT^2 at various fields $0.03 < B/|K| < 0.73$ with a fixed angle $\theta = 0.8^\circ$ on the $YC4 \times 6 \times 2$ lattice. The curves are shifted vertically by a value of 0.1 in (a), a value of 5 in (b), and 100 in (c) for clarity. The characteristic temperature scales T_H , T_L , T_L' , and T_L'' are indicated by the arrows.

and the magnetic susceptibility χ in the case under a field of $B/|K| = 0.38$ tilted by an angle $\theta = 0.8^\circ$. In Fig. 5(a), we find the thermal entropy releases in two steps near the high-temperature scale T_H and the low-temperature scale T_L'' . T_H corresponds to the establishment of short-range spin correlations while T_L'' to the alignment of W_p . Between T_H and T_L'' there resides a KFL regime. Below T_L'' , a gapless QSL has been proposed [32] whose precise nature is still under investigation [42]. As shown in Fig. 5(b), the magnetic

susceptibility exhibits an emergent Curie-Weiss law (with constants different from the high-temperature Curie-Weiss behavior) in the intermediate-temperature regime. With universal signatures in thermodynamics [32,47], we identify that the KFL behaviors still exist under tilted fields.

In Fig. 6, we plot the specific heat C_m curves and their first- and second-order derivatives dC_m/dT and d^2C_m/dT^2 under various fields $B/|K|$ with a fixed angle $\theta = 0.8^\circ$. The temperature scales T_H , T_L , and T_L'' could be determined from the hump/shoulder positions in Fig. 6(a), or from the derivatives $dC_m/dT = 0$ in Fig. 6(b). As for the shoulder feature at T_L' , we identified that scale from the second-order derivatives d^2C_m/dT^2 as shown in Fig. 6(c), where the largest absolute value corresponds to a minimal curvature. In Fig. 2(a) of the main text, we plot the tendency of the characteristic temperature scales by the dashed lines, which connects smoothly to the quantum phase transition points obtained from the ground-state DMRG calculations [30].

APPENDIX B: EXPONENTIAL TENSOR RENORMALIZATION GROUP METHOD

The exponential tensor renormalization group (XTRG) method [33,34] exploited in this work carries out the finite-temperature many-body simulations down to low temperature exponentially fast, which has been shown to be a highly efficient and very powerful tool in solving various two-dimensional (2D) spin lattice models [34,35,47,92], realistic quantum magnets [32,93–95], and correlated fermion system [96,97]. Below we synopsise the main idea of such a method and provide some benchmark results on the realistic K - J - Γ - Γ' model.

In XTRG, we start with the high-temperature density matrix $\rho(\tau_0)$ with the initial $\tau_0 \equiv |K|/T = 0.0025$ through a series expansion in thermal tensor networks [33], i.e.,

$$\rho(\tau_0) = e^{-\tau_0 \hat{H}} \simeq \sum_{n=0}^{N_c} \frac{(-\tau_0)^n}{n!} \hat{H}^n, \quad (\text{B1})$$

where N_c is the expansion order (often smaller than 10 in practice) and the $\rho(\tau_0)$ could converge to machine precision. Given the density matrix $\rho(\tau_0)$ represented in the form of a matrix product operator (MPO), we keep squaring the MPO via tensor network contractions and thus cool down the system exponentially as $\rho(\tau_n) = \rho(\tau_{n-1}) \cdot \rho(\tau_{n-1})$ where $\tau_n = 2^n \tau_0$ ($n \geq 1$). Based on this, various thermodynamic properties can be computed, including free energy f , internal energy u , magnetic thermal entropy S , static spin-structure factors $S(\mathbf{k})$, and so on. We perform in parallel the simulations with interleaved data points along the temperature axis and interpolate data between those sampling points.

For the $YC4 \times 6 \times 2$ geometry considered in the main text, we compare in Fig. 7 the low-temperature magnetization curves ($\theta = 0.8^\circ$ case) calculated by the XTRG method with the DMRG results [30], where we find the $T/|K| = 0.0085$ data converge well with the DMRG data. This confirms that the XTRG calculations can approach the low-temperature regime in close vicinity of the ground state.

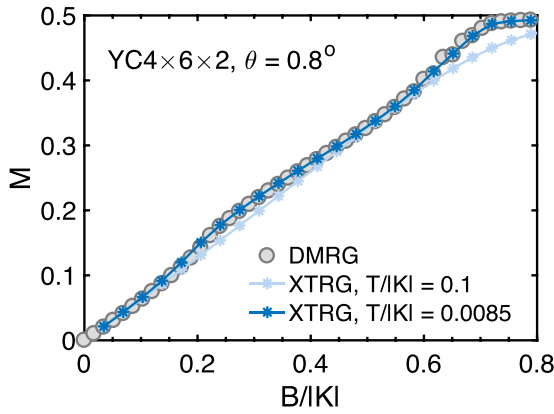


FIG. 7. The low-temperature magnetization curves with field applied along $\theta = 0.8^\circ$ of the α -RuCl₃ model. When the temperature is sufficiently low, the results converge to the ground-state curve computed with DMRG [30] on the same YC4 \times 6 \times 2 geometry.

APPENDIX C: MATRIX PRODUCT OPERATOR ENTANGLEMENT

The phase transitions can be detected sensitively by the entanglement entropy of the matrix product operator (MPO) [34]. Regarding the MPO as a supervector, we can take a Schmidt decomposition of the purified “wave function” and compute the entanglement entropy S_E between the two parts of the system. Here we study its field-dependent behaviors for $\theta = 0.8^\circ$ and 5° , on the YC4 \times 6 \times 2 lattice with the calculated results shown in Fig. 8.

The MPO entanglement entropy S_E is expected to diverge at the second-order quantum critical point (QCP) in the low-temperature limit. In finite-size calculations, it instead exhibits

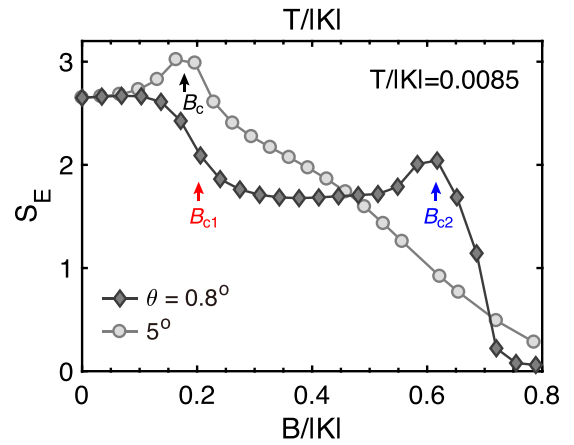


FIG. 8. The bipartite MPO entanglement entropies S_E under various fields B applied along $\theta = 0.8^\circ$ and $\theta = 5^\circ$, at a low temperature $T/|K| = 0.0085$. A drop and a peak features can be seen at, respectively, the low and high transition fields B_{c1} and B_{c2} for $\theta = 0.8^\circ$ (denoted by the red and blue arrows). For the $\theta = 5^\circ$ case, there is only a single peak in the S_E curve located at B_c .

a peak near the QCP. In Fig. 8, we show the low-temperature S_E versus magnetic fields B and find for the $\theta = 0.8^\circ$ case there exists a peak near B_{c2} . This is indicated by the blue arrow, with the determined field value consistent with that obtained from Γ_B data in Fig. 2(e). In addition, it can be seen that S_E first shows an almost steady behavior at the low-field antiferromagnetic phase, then drops abruptly near B_{c1} as indicated by the red arrow, reflecting that the low-field phase transition is likely of first order. For the $\theta = 5^\circ$ case, there is only a single peak for S_E versus B as shown in Fig. 8, where a prominent peak at B_c clearly signals the QCP between the zigzag and spin-polarized phases.

-
- [1] P. W. Anderson, Resonating valence bonds: A new kind of insulator? *Mater. Res. Bull.* **8**, 153 (1973).
- [2] L. Balents, Spin liquids in frustrated magnets, *Nature (London)* **464**, 199 (2010).
- [3] Y. Zhou, K. Kanoda, and T.-K. Ng, Quantum spin liquid states, *Rev. Mod. Phys.* **89**, 025003 (2017).
- [4] J. Wen, S.-L. Yu, S. Li, W. Yu, and J.-X. Li, Experimental identification of quantum spin liquids, *npj Quantum Mater.* **4**, 12 (2019).
- [5] C. Broholm, R. J. Cava, S. A. Kivelson, D. G. Nocera, M. R. Norman, and T. Senthil, Quantum spin liquids, *Science* **367**, eaay0668 (2020).
- [6] A. Kitaev, Fault-tolerant quantum computation by anyons, *Ann. Phys. (NY)* **303**, 2 (2003).
- [7] A. Kitaev, Anyons in an exactly solved model and beyond, *Ann. Phys. (NY)* **321**, 2 (2006).
- [8] G. Jackeli and G. Khaliullin, Mott Insulators in the Strong Spin-Orbit Coupling Limit: From Heisenberg to a Quantum Compass and Kitaev Models, *Phys. Rev. Lett.* **102**, 017205 (2009).
- [9] S. Trebst, Kitaev materials, *arXiv:1701.07056*.
- [10] S. M. Winter, A. A. Tsirlin, M. Daghofer, J. van den Brink, Y. Singh, P. Gegenwart, and R. Valentí, Models and materials for generalized Kitaev magnetism, *J. Phys.: Condens. Matter* **29**, 493002 (2017).
- [11] L. Janssen and M. Vojta, Heisenberg–Kitaev physics in magnetic fields, *J. Phys.: Condens. Matter* **31**, 423002 (2019).
- [12] Y. Motome, R. Sano, S. Jang, Y. Sugita, and Y. Kato, Materials design of Kitaev spin liquids beyond the Jackeli-Khaliullin mechanism, *J. Phys.: Condens. Matter* **32**, 404001 (2020).
- [13] J. A. Sears, M. Songvilay, K. W. Plumb, J. P. Clancy, Y. Qiu, Y. Zhao, D. Parshall, and Y.-J. Kim, Magnetic order in α -RuCl₃: A honeycomb-lattice quantum magnet with strong spin-orbit coupling, *Phys. Rev. B* **91**, 144420 (2015).
- [14] A. Banerjee, J. Yan, J. Knolle, C. A. Bridges, M. B. Stone, M. D. Lumsden, D. G. Mandrus, D. A. Tennant, R. Moessner, and S. E. Nagler, Neutron scattering in the proximate quantum spin liquid α -RuCl₃, *Science* **356**, 1055 (2017).
- [15] S.-H. Do, S.-Y. Park, J. Yoshitake, J. Nasu, Y. Motome, Y. S. Kwon, D. T. Adroja, D. J. Voneshen, K. Kim, T.-H. Jang, J.-H. Park, K.-Y. Choi, and S. Ji, Majorana fermions in the Kitaev quantum spin system α -RuCl₃, *Nat. Phys.* **13**, 1079 (2017).
- [16] A. Banerjee, P. Lampen-Kelley, J. Knolle, C. Balz, A. Aczel, B. Winn, Y. Liu, D. Pajerowski, J. Yan, C. A. Bridges, A. T. Savici, B. C. Chakoumakos, M. D. Lumsden, D. A. Tennant, R.

- Moessner, D. G. Mandrus, and S. E. Nagler, Excitations in the field-induced quantum spin liquid state of α -RuCl₃, *npj Quant. Mater.* **3**, 8 (2018).
- [17] C. Balz, L. Janssen, P. Lampen-Kelley, A. Banerjee, Y. H. Liu, J.-Q. Yan, D. G. Mandrus, M. Vojta, and S. E. Nagler, Field-induced intermediate ordered phase and anisotropic interlayer interactions in α -RuCl₃, *Phys. Rev. B* **103**, 174417 (2021).
- [18] J. A. Sears, Y. Zhao, Z. Xu, J. W. Lynn, and Y.-J. Kim, Phase diagram of α -RuCl₃ in an in-plane magnetic field, *Phys. Rev. B* **95**, 180411(R) (2017).
- [19] J. Zheng, K. Ran, T. Li, J. Wang, P. Wang, B. Liu, Z.-X. Liu, B. Normand, J. Wen, and W. Yu, Gapless Spin Excitations in the Field-Induced Quantum Spin Liquid Phase of α -RuCl₃, *Phys. Rev. Lett.* **119**, 227208 (2017).
- [20] S.-H. Baek, S.-H. Do, K.-Y. Choi, Y. S. Kwon, A. U. B. Wolter, S. Nishimoto, J. van den Brink, and B. Büchner, Evidence for a Field-Induced Quantum Spin Liquid in α -RuCl₃, *Phys. Rev. Lett.* **119**, 037201 (2017).
- [21] N. Janša, A. Zorko, M. Gomilšek, M. Pregelj, K. W. Krämer, D. Biner, A. Biffin, C. Rüegg, and M. Klanjšek, Observation of two types of fractional excitation in the Kitaev honeycomb magnet, *Nat. Phys.* **14**, 786 (2018).
- [22] D. Wulferding, Y. Choi, S.-H. Do, C. H. Lee, P. Lemmens, C. Faugeras, Y. Gallais, and K.-Y. Choi, Magnon bound states versus anyonic Majorana excitations in the Kitaev honeycomb magnet α -RuCl₃, *Nat. Commun.* **11**, 1603 (2020).
- [23] A. N. Ponomaryov, L. Zviagina, J. Wosnitzer, P. Lampen-Kelley, A. Banerjee, J.-Q. Yan, C. A. Bridges, D. G. Mandrus, S. E. Nagler, and S. A. Zvyagin, Nature of Magnetic Excitations in the High-Field Phase of α -RuCl₃, *Phys. Rev. Lett.* **125**, 037202 (2020).
- [24] I. A. Leahy, C. A. Pocs, P. E. Siegfried, D. Graf, S.-H. Do, K.-Y. Choi, B. Normand, and M. Lee, Anomalous Thermal Conductivity and Magnetic Torque Response in the Honeycomb Magnet α -RuCl₃, *Phys. Rev. Lett.* **118**, 187203 (2017).
- [25] K. A. Modic, R. D. McDonald, J. P. C. Ruff, M. D. Bachmann, Y. Lai, J. C. Palmstrom, D. Graf, M. K. Chan, F. F. Balakirev, J. B. Betts, G. S. Boebinger, M. Schmidt, M. J. Lawler, D. A. Sokolov, P. J. W. Moll, B. J. Ramshaw, and A. Shekhter, Scale-invariant magnetic anisotropy in RuCl₃ at high magnetic fields, *Nat. Phys.* **17**, 240 (2021).
- [26] Y. Kasahara, K. Sugii, T. Ohnishi, M. Shimozawa, M. Yamashita, N. Kurita, H. Tanaka, J. Nasu, Y. Motome, T. Shibauchi, and Y. Matsuda, Unusual Thermal Hall Effect in a Kitaev Spin Liquid Candidate α -RuCl₃, *Phys. Rev. Lett.* **120**, 217205 (2018).
- [27] Y. Kasahara, T. Ohnishi, Y. Mizukami, O. Tanaka, S. Ma, K. Sugii, N. Kurita, H. Tanaka, J. Nasu, Y. Motome, T. Shibauchi, and Y. Matsuda, Majorana quantization and half-integer thermal quantum Hall effect in a Kitaev spin liquid, *Nature (London)* **559**, 227 (2018).
- [28] T. Yokoi, S. Ma, Y. Kasahara, S. Kasahara, T. Shibauchi, N. Kurita, H. Tanaka, J. Nasu, Y. Motome, C. Hickey, S. Trebst, and Y. Matsuda, Half-integer quantized anomalous thermal Hall effect in the Kitaev material candidate α -RuCl₃, *Science* **373**, 568 (2021).
- [29] M. Yamashita, J. Gouchi, Y. Uwatoko, N. Kurita, and H. Tanaka, Sample dependence of half-integer quantized thermal Hall effect in the Kitaev spin-liquid candidate α -RuCl₃, *Phys. Rev. B* **102**, 220404(R) (2020).
- [30] X.-G. Zhou, H. Li, Y. H. Matsuda, A. Matsuo, W. Li, N. Kurita, K. Kindo, and H. Tanaka, Intermediate Quantum Spin Liquid Phase in the Kitaev Material α -RuCl₃ under High Magnetic Fields up to 100 T, *arXiv:2201.04597*.
- [31] P. Laurell and S. Okamoto, Dynamical and thermal magnetic properties of the Kitaev spin liquid candidate α -RuCl₃, *npj Quant. Mater.* **5**, 2 (2020).
- [32] H. Li, H.-K. Zhang, J. Wang, H.-Q. Wu, Y. Gao, D.-W. Qu, Z.-X. Liu, S.-S. Gong, and W. Li, Identification of magnetic interactions and high-field quantum spin liquid in α -RuCl₃, *Nat. Commun.* **12**, 4007 (2021).
- [33] B.-B. Chen, Y.-J. Liu, Z. Chen, and W. Li, Series-expansion thermal tensor network approach for quantum lattice models, *Phys. Rev. B* **95**, 161104(R) (2017).
- [34] B.-B. Chen, L. Chen, Z. Chen, W. Li, and A. Weichselbaum, Exponential Thermal Tensor Network Approach for Quantum Lattice Models, *Phys. Rev. X* **8**, 031082 (2018).
- [35] H. Li, B.-B. Chen, Z. Chen, J. von Delft, A. Weichselbaum, and W. Li, Thermal tensor renormalization group simulations of square-lattice quantum spin models, *Phys. Rev. B* **100**, 045110 (2019).
- [36] Y. Kubota, H. Tanaka, T. Ono, Y. Narumi, and K. Kindo, Successive magnetic phase transitions in α -RuCl₃: XY-like frustrated magnet on the honeycomb lattice, *Phys. Rev. B* **91**, 094422 (2015).
- [37] S. Widmann, V. Tsurkan, D. A. Prishchenko, V. G. Mazurenko, A. A. Tsirlin, and A. Loidl, Thermodynamic evidence of fractionalized excitations in α -RuCl₃, *Phys. Rev. B* **99**, 094415 (2019).
- [38] R. D. Johnson, S. C. Williams, A. A. Haghighirad, J. Singleton, V. Zapf, P. Manuel, I. I. Mazin, Y. Li, H. O. Jeschke, R. Valentí, and R. Coldea, Monoclinic crystal structure of α -RuCl₃ and the zigzag antiferromagnetic ground state, *Phys. Rev. B* **92**, 235119 (2015).
- [39] D. Weber, L. M. Schoop, V. Duppl, J. M. Lippmann, J. Nuss, and B. V. Lotsch, Magnetic Properties of Restacked 2D Spin 1/2 honeycomb RuCl₃ Nanosheets, *Nano Lett.* **16**, 3578 (2016).
- [40] P. Lampen-Kelley, S. Rachel, J. Reuther, J.-Q. Yan, A. Banerjee, C. A. Bridges, H. B. Cao, S. E. Nagler, and D. Mandrus, Anisotropic susceptibilities in the honeycomb Kitaev system α -RuCl₃, *Phys. Rev. B* **98**, 100403(R) (2018).
- [41] J. A. Sears, L. E. Chern, S. Kim, P. J. Bereciartua, S. Francoual, Y. B. Kim, and Y.-J. Kim, Ferromagnetic Kitaev interaction and the origin of large magnetic anisotropy in α -RuCl₃, *Nat. Phys.* **16**, 837 (2020).
- [42] S. Yu, H. Li, Q.-R. Zhao, W. Li, Z.-X. Liu, and S.-S. Gong, Nematicity and Intermediate Quantum Spin Liquid Phase in the K - J - Γ - Γ' model (unpublished).
- [43] J. Nasu, M. Udagawa, and Y. Motome, Vaporization of Kitaev Spin Liquids, *Phys. Rev. Lett.* **113**, 197205 (2014).
- [44] J. Nasu, M. Udagawa, and Y. Motome, Thermal fractionalization of quantum spins in a Kitaev model: Temperature-linear specific heat and coherent transport of majorana fermions, *Phys. Rev. B* **92**, 115122 (2015).
- [45] J. Yoshitake, J. Nasu, and Y. Motome, Fractional Spin Fluctuations as a Precursor of Quantum Spin Liquids: Majorana Dynamical Mean-Field Study for the Kitaev Model, *Phys. Rev. Lett.* **117**, 157203 (2016).
- [46] J. Yoshitake, J. Nasu, and Y. Motome, Temperature evolution of spin dynamics in two- and three-dimensional Kitaev mod-

- els: Influence of fluctuating Z_2 flux, *Phys. Rev. B* **96**, 064433 (2017).
- [47] H. Li, D.-W. Qu, H.-K. Zhang, Y.-Z. Jia, S.-S. Gong, Y. Qi, and W. Li, Universal thermodynamics in the Kitaev fractional liquid, *Phys. Rev. Res.* **2**, 043015 (2020).
- [48] S. Bachus, D. A. S. Kaib, A. Jesche, V. Tsurkan, A. Loidl, S. M. Winter, A. A. Tsirlin, R. Valentí, and P. Gegenwart, Angle-dependent thermodynamics of α -RuCl₃, *Phys. Rev. B* **103**, 054440 (2021).
- [49] K. A. Modic, M. D. Bachmann, B. J. Ramshaw, F. Arnold, K. R. Shirer, A. Estry, J. B. Betts, N. J. Ghimire, E. D. Bauer, M. Schmidt, M. Baenitz, E. Svanidze, R. D. McDonald, A. Shekhter, and P. J. W. Moll, Resonant torsion magnetometry in anisotropic quantum materials, *Nat. Commun.* **9**, 3975 (2018).
- [50] A. Shekhter, R. D. McDonald, B. J. Ramshaw, and K. A. Modic, The magnetotropic susceptibility, [arXiv:2208.10038](https://arxiv.org/abs/2208.10038).
- [51] Y. Singh and P. Gegenwart, Antiferromagnetic Mott insulating state in single crystals of the honeycomb lattice material Na₂IrO₃, *Phys. Rev. B* **82**, 064412 (2010).
- [52] J. Chaloupka, G. Jackeli, and G. Khaliullin, Kitaev-Heisenberg Model on a Honeycomb Lattice: Possible Exotic Phases in Iridium Oxides A₂IrO₃, *Phys. Rev. Lett.* **105**, 027204 (2010).
- [53] Y. Singh, S. Manni, J. Reuther, T. Berlijn, R. Thomale, W. Ku, S. Trebst, and P. Gegenwart, Relevance of the Heisenberg-Kitaev Model for the Honeycomb Lattice Iridates A₂IrO₃, *Phys. Rev. Lett.* **108**, 127203 (2012).
- [54] V. M. Katukuri, S. Nishimoto, V. Yushankhai, A. Stoyanova, H. Kandpal, S. Choi, R. Coldea, I. Rousochatzakis, L. Hozoi, and J. van den Brink, Kitaev interactions between $J = 1/2$ moments in honeycomb Na₂IrO₃ are large and ferromagnetic: Insights from *ab initio* quantum chemistry calculations, *New J. Phys.* **16**, 013056 (2014).
- [55] Y. Yamaji, Y. Nomura, M. Kurita, R. Arita, and M. Imada, First-Principles Study of the Honeycomb-Lattice Iridates Na₂IrO₃ in the Presence of Strong Spin-Orbit Interaction and Electron Correlations, *Phys. Rev. Lett.* **113**, 107201 (2014).
- [56] S. M. Winter, Y. Li, H. O. Jeschke, and R. Valentí, Challenges in design of Kitaev materials: Magnetic interactions from competing energy scales, *Phys. Rev. B* **93**, 214431 (2016).
- [57] K. Mehlawat, A. Thamizhavel, and Y. Singh, Heat capacity evidence for proximity to the Kitaev quantum spin liquid in A₂IrO₃ (A = Na, Li), *Phys. Rev. B* **95**, 144406 (2017).
- [58] M. Abramchuk, C. Ozsoy-Keskinbora, J. W. Krizan, K. R. Metz, D. C. Bell, and F. Tafti, Cu₂IrO₃: A new magnetically frustrated honeycomb iridate, *J. Am. Chem. Soc.* **139**, 15371 (2017).
- [59] Y. S. Choi, C. H. Lee, S. Lee, S. Yoon, W.-J. Lee, J. Park, A. Ali, Y. Singh, J.-C. Orain, G. Kim, J.-S. Rhyee, W.-T. Chen, F. Chou, and K.-Y. Choi, Exotic Low-Energy Excitations Emergent in the Random Kitaev Magnet Cu₂IrO₃, *Phys. Rev. Lett.* **122**, 167202 (2019).
- [60] V. Todorova, A. Leineweber, L. Kienle, V. Duppel, and M. Jansen, On AgRhO₂, and the new quaternary delafossites AgLi_{1/3} M_{2/3} O₂, syntheses and analyses of real structures, *J. Solid State Chem.* **184**, 1112 (2011).
- [61] J. H. Roudebush, K. A. Ross, and R. J. Cava, Iridium containing honeycomb delafossites by topotactic cation exchange, *Dalton Trans.* **45**, 8783 (2016).
- [62] K. Kitagawa, T. Takayama, Y. Matsumoto, A. Kato, R. Takano, Y. Kishimoto, S. Bette, R. Dinnebier, G. Jackeli, and H. Takagi, A spin-orbital-entangled quantum liquid on a honeycomb lattice, *Nature (London)* **554**, 341 (2018).
- [63] S. M. Winter, K. Riedl, P. A. Maksimov, A. L. Chernyshev, A. Honecker, and R. Valentí, Breakdown of magnons in a strongly spin-orbital coupled magnet, *Nat. Commun.* **8**, 1152 (2017).
- [64] L. Wu, A. Little, E. E. Aldape, D. Rees, E. Thewalt, P. Lampen-Kelley, A. Banerjee, C. A. Bridges, J.-Q. Yan, D. Boone, S. Patankar, D. Goldhaber-Gordon, D. Mandrus, S. E. Nagler, E. Altman, and J. Orenstein, Field evolution of magnons in α -RuCl₃ by high-resolution polarized terahertz spectroscopy, *Phys. Rev. B* **98**, 094425 (2018).
- [65] T. Cookmeyer and J. E. Moore, Spin-wave analysis of the low-temperature thermal Hall effect in the candidate Kitaev spin liquid α -RuCl₃, *Phys. Rev. B* **98**, 060412(R) (2018).
- [66] H.-S. Kim and H.-Y. Kee, Crystal structure and magnetism in α -RuCl₃: An *ab initio* study, *Phys. Rev. B* **93**, 155143 (2016).
- [67] T. Suzuki and S.-I. Suga, Erratum: Effective model with strong Kitaev interactions for α -RuCl₃ [*Phys. Rev. B* **97**, 134424 (2018)], *Phys. Rev. B* **99**, 249902(E) (2019).
- [68] K. Ran, J. Wang, W. Wang, Z.-Y. Dong, X. Ren, S. Bao, S. Li, Z. Ma, Y. Gan, Y. Zhang, J. T. Park, G. Deng, S. Danilkin, S.-L. Yu, J.-X. Li, and J. Wen, Spin-wave excitations evidencing the Kitaev interaction in single crystalline α -RuCl₃, *Phys. Rev. Lett.* **118**, 107203 (2017).
- [69] W. Wang, Z.-Y. Dong, S.-L. Yu, and J.-X. Li, Theoretical investigation of magnetic dynamics in α -RuCl₃, *Phys. Rev. B* **96**, 115103 (2017).
- [70] I. O. Ozel, C. A. Belvin, E. Baldini, I. Kimchi, S.-H. Do, K.-Y. Choi, and N. Gedik, Magnetic field-dependent low-energy magnon dynamics in α -RuCl₃, *Phys. Rev. B* **100**, 085108 (2019).
- [71] A. Banerjee, C. A. Bridges, J. Q. Yan, A. A. Aczel, L. Li, M. B. Stone, G. E. Granroth, M. D. Lumsden, Y. Yiu, J. Knolle, S. Bhattacharjee, D. L. Kovrizhin, R. Moessner, D. A. Tennant, D. G. Mandrus, and S. E. Nagler, Proximate Kitaev quantum spin liquid behaviour in a honeycomb magnet, *Nat. Mater.* **15**, 733 (2016).
- [72] H.-S. Kim, Vijay Shankar V., A. Catuneanu, and H.-Y. Kee, Kitaev magnetism in honeycomb RuCl₃ with intermediate spin-orbit coupling, *Phys. Rev. B* **91**, 241110(R) (2015).
- [73] D. Ni, X. Gui, K. M. Powderly, and R. J. Cava, Honeycomb-structure RuI₃, a new quantum material related to α -RuCl₃, *Adv. Mater.* **34**, 2106831 (2022).
- [74] Y. Imai, K. Nawa, Y. Shimizu, W. Yamada, H. Fujihara, T. Aoyama, R. Takahashi, D. Okuyama, T. Ohashi, M. Hagihala, S. Torii, D. Morikawa, M. Terauchi, T. Kawamata, M. Kato, H. Gotou, M. Itoh, T. J. Sato, and K. Ohgushi, Zigzag magnetic order in the Kitaev spin-liquid candidate material RuBr₃ with a honeycomb lattice, *Phys. Rev. B* **105**, L041112 (2022).
- [75] Y. Hao, H. Wo, Y. Gu, X. Zhang, Y. Gu, S. Zheng, Y. Zhao, G. Xu, J. W. Lynn, K. Nakajima, N. Murai, W. Wang, and J. Zhao, Field-tuned magnetic structure and phase diagram of the honeycomb magnet YbCl₃, *Sci. China Phys. Mech. Astron.* **64**, 237411 (2021).
- [76] J. Xing, E. Feng, Y. Liu, E. Emmanouilidou, C. Hu, J. Liu, D. Graf, A. P. Ramirez, G. Chen, H. Cao, and N. Ni, Néel-type antiferromagnetic order and magnetic field-temperature phase diagram in the spin- $\frac{1}{2}$ rare-earth honeycomb compound YbCl₃, *Phys. Rev. B* **102**, 014427 (2020).

- [77] G. Sala, M. B. Stone, B. K. Rai, A. F. May, P. Laurell, V. O. Garlea, N. P. Butch, M. D. Lumsden, G. Ehlers, G. Pokharel, D. Mandrus, D. S. Parker, S. Okamoto, G. B. Halász, and A. D. Christianson, Van Hove singularity in the magnon spectrum of the antiferromagnetic quantum honeycomb lattice, [arXiv:2003.01754](https://arxiv.org/abs/2003.01754).
- [78] M. A. McGuire, H. Dixit, V. R. Cooper, and B. C. Sales, Coupling of crystal structure and magnetism in the layered, ferromagnetic insulator CrI_3 , *Chem. Mater.* **27**, 612 (2015).
- [79] J. Ji, M. Sun, Y. Cai, Y. Wang, Y. Sun, W. Ren, Z. Zhang, F. Jin, and Q. Zhang, Rare-Earth Chalcogenides: A Family of van der Waals Layered Kitaev Spin Liquid Candidates, *Chinese Phys. Lett.* **38**, 047502 (2021).
- [80] Z. Zhang, Y. Cai, J. Kang, Z. Ouyang, Z. Zhang, A. Zhang, J. Ji, F. Jin, and Q. Zhang, Anisotropic exchange coupling and ground state phase diagram of Kitaev compound YbOCl , *Phys. Rev. Res.* **4**, 033006 (2022).
- [81] G. Lin, J. Jeong, C. Kim, Y. Wang, Q. Huang, T. Masuda, S. Asai, S. Itoh, G. Günther, M. Russina, Z. Lu, J. Sheng, L. Wang, J. Wang, G. Wang, Q. Ren, C. Xi, W. Tong, L. Ling, Z. Liu *et al.*, Field-induced quantum spin disordered state in spin-1/2 honeycomb magnet $\text{Na}_2\text{Co}_2\text{TeO}_6$, *Nat. Commun.* **12**, 5559 (2021).
- [82] W. Yao, K. Iida, K. Kamazawa, and Y. Li, Excitations in the ordered and paramagnetic states of honeycomb magnet $\text{Na}_2\text{Co}_2\text{TeO}_6$, *Phys. Rev. Lett.* **129**, 147202 (2022).
- [83] H. Liu, J. Chaloupka, and G. Khaliullin, Kitaev spin liquid in 3d transition metal compounds, *Phys. Rev. Lett.* **125**, 047201 (2020).
- [84] R. Zhong, T. Gao, N. P. Ong, and R. J. Cava, Weak-field induced nonmagnetic state in a Co-based honeycomb, *Sci. Adv.* **6**, eaay6953 (2020).
- [85] K. W. Plumb, J. P. Clancy, L. J. Sandilands, V. V. Shankar, Y. F. Hu, K. S. Burch, H.-Y. Kee, and Y.-J. Kim, α - RuCl_3 : A spin-orbit assisted Mott insulator on a honeycomb lattice, *Phys. Rev. B* **90**, 041112(R) (2014).
- [86] L. Janssen, E. C. Andrade, and M. Vojta, Magnetization processes of zigzag states on the honeycomb lattice: Identifying spin models for α - RuCl_3 and Na_2IrO_3 , *Phys. Rev. B* **96**, 064430 (2017).
- [87] E. C. Andrade, L. Janssen, and M. Vojta, Susceptibility anisotropy and its disorder evolution in models for Kitaev materials, *Phys. Rev. B* **102**, 115160 (2020).
- [88] P. M. Cönsoli and E. C. Andrade, Stability of ordered and disordered phases in the Heisenberg-Kitaev model in a magnetic field, *J. Phys.: Conf. Ser.* **2164**, 012024 (2022).
- [89] J. Yoshitake, J. Nasu, Y. Kato, and Y. Motome, Majorana-magnon crossover by a magnetic field in the Kitaev model: Continuous-time quantum Monte Carlo study, *Phys. Rev. B* **101**, 100408(R) (2020).
- [90] J. S. Gordon, A. Catuneanu, E. S. Sørensen, and H.-Y. Kee, Theory of the field-revealed Kitaev spin liquid, *Nat. Commun.* **10**, 2470 (2019).
- [91] H.-Y. Lee, R. Kaneko, L. E. Chern, T. Okubo, Y. Yamaji, N. Kawashima, and Y. B. Kim, Magnetic field induced quantum phases in a tensor network study of Kitaev magnets, *Nat. Commun.* **11**, 1639 (2020).
- [92] L. Chen, D.-W. Qu, H. Li, B.-B. Chen, S.-S. Gong, J. von Delft, A. Weichselbaum, and W. Li, Two temperature scales in the triangular lattice Heisenberg antiferromagnet, *Phys. Rev. B* **99**, 140404(R) (2019).
- [93] H. Li, Y.-D. Liao, B.-B. Chen, X.-T. Zeng, X.-L. Sheng, Y. Qi, Z. Y. Meng, and W. Li, Kosterlitz-Thouless melting of magnetic order in the triangular quantum Ising material TmMgGaO_4 , *Nat. Commun.* **11**, 1111 (2020).
- [94] Z. Hu, Z. Ma, Y.-D. Liao, H. Li, C. Ma, Y. Cui, Y. Shangguan, Z. Huang, Y. Qi, W. Li, Z. Y. Meng, J. Wen, and W. Yu, Evidence of the Berezinskii-Kosterlitz-Thouless phase in a frustrated magnet, *Nat. Commun.* **11**, 5631 (2020).
- [95] Y. Gao, Y.-C. Fan, H. Li, F. Yang, X.-T. Zeng, X.-L. Sheng, R. Zhong, Y. Qi, Y. Wan, and W. Li, Spin supersolidity in nearly ideal easy-axis triangular quantum antiferromagnet $\text{Na}_2\text{BaCo}(\text{PO}_4)_2$, *npj Quant. Mater.* **7**, 89 (2022).
- [96] B.-B. Chen, C. Chen, Z. Chen, J. Cui, Y. Zhai, A. Weichselbaum, J. von Delft, Z. Y. Meng, and W. Li, Quantum many-body simulations of the two-dimensional Fermi-Hubbard model in ultracold optical lattices, *Phys. Rev. B* **103**, L041107 (2021).
- [97] X. Lin, B.-B. Chen, W. Li, Z. Y. Meng, and T. Shi, Exciton Proliferation and Fate of the Topological Mott Insulator in a Twisted Bilayer Graphene Lattice Model, *Phys. Rev. Lett.* **128**, 157201 (2022).